SCIENTIFIC REPORTS

OPEN

SUBJECT AREAS:
ELECTRONIC MATERIALS AND DEVICES
MATERIALS CHEMISTRY
METHODS
INORGANIC CHEMISTRY

Received
25 June 2012

Accepted
13 August 2012

Published
30 August 2012

Correspondence and requests for materials should be addressed to S.-H.Y. (shyu@ustc.edu.cn)

Wet-spinning assembly of continuous, neat, and macroscopic graphene fibers

Huai-Ping Cong, Xiao-Chen Ren, Ping Wang & Shu-Hong Yu

Division of Nanomaterials and Chemistry, Hefei National Laboratory for Physical Sciences at Microscale, Department of Chemistry, Department of Materials Science and Engineering, the National Synchrotron Radiation Laboratory, University of Science and Technology of China, Hefei, Anhui 230026, P. R. China.

Graphene is now the most attractive carbon-based material. Integration of 2D graphene sheets into macroscopic architectures such as fibers illuminates the direction to translate the excellent properties of individual graphene into advanced hierarchical ensembles for promising applications in new graphene-based nanodevices. However, the lack of effective, low-cost and convenient assembly strategy has blocked its further development. Herein, we demonstrate that neat and macroscopic graphene fibers with high mechanical strength and electrical conductivity can be fluidly spun from the common graphene oxide (GO) suspensions in large scale followed with chemical reduction. The curliness-fold formation mechanism of GO fiber has been proposed. This wet-spinning technique presented here facilitates the multifunctionalization of macroscopic graphene-based fibers with various organic or inorganic components by an easy-handle *in situ* or post-synthesis approach, which builds the solid foundation to access a new family of advanced composite materials for the next practical applications.

Graphene, a two-dimension (2D) monolayer of sp^2-hybridized carbon atoms tightly packed into a honeycomb lattice[1], the fundamental building block of all the graphitic materials, has attracted persistent attention. The intriguing electronic, thermal, and mechanic properties[2–3] mainly arise from its truly atomic thickness and strictly 2D structure, and therefore bring about the greatly promising applications in electronic and energy storage devices[4–5], sensors[6–7], catalysis[8–9], composites[10] and so on.

Nowadays, translation of the individual property of the graphene sheets into the macroscopic, ordered materials is without doubt an extraordinarily hot and useful topic in view of exploring advanced properties of 2D graphene sheets for practical applications. Fruitful progresses have demonstrated that graphene sheets can be assembled into 2D macroscopic thin films[11–15], and 3D composites with polymers[16–18] or hydrogel-structured monoliths[19–22] via various methods and techniques. However, in most cases, the limited dispersibility of graphene sheets in common solvents hinders the development of the direct assembly of graphene sheets.

Alternatively, graphene oxide (GO) with abundant of oxygen functional groups on its basal planes and edges is accessible to be completely exfoliated and form colloidal dispersions of single sheets in water and other polar organic solvents. The advantages of GO, such as good solubility, easy handle, and scalable production with low cost improve the chances in assembling 2D sheets into macroscopic graphene-based architectures. Even though, very few reports have been made on the macroscopically finely-assembled graphene fibers with high concentrated liquid crystalline graphene oxide[23], or by a complex dimensionally-confined hydrothermal strategy[24], mainly due to the asymmetric sizes and irregular shapes of graphene sheets, as well as the lack of the effective assembly method. In comparison, macroscopic fibers of carbon nanotubes have been well assembled through wet spinning of single-walled nanotubes[25–27] and dry-state spinning of multi-walled nanotubes[28–30]. However, it can not be ignored that accompanying with the excellent properties of the assemblies, the high costs of the superaligned carbon tube arrays or strict conditions have to be involved into assembling these neat carbon-nanotube fibers. Based on this point, without weakening properties of the as-products, but solving the disadvantages for assembly of carbon tubes, it is urgent to develop an effective, easy-handle and fast method to assemble the alternative graphene sheets into macroscopic fibers in a controllable, uniform and large-scale manner for potential applications.

Herein, we report a facile fluid assembly approach to produce macroscopic, neat and large-scale graphene fibers by processing GO solutions via a simple and effective wet-spinning technique followed with the chemical reduction. Furthermore, for the fist time, we clarified the assembly mechanism of the GO sheets into macroscopic fibers by spinning of the GO dispersion in a coagulation bath of the hexadecyltrimethyl ammonium bromide (CTAB) solution with a low concentration. The as-prepared graphene fibers were possessed with good

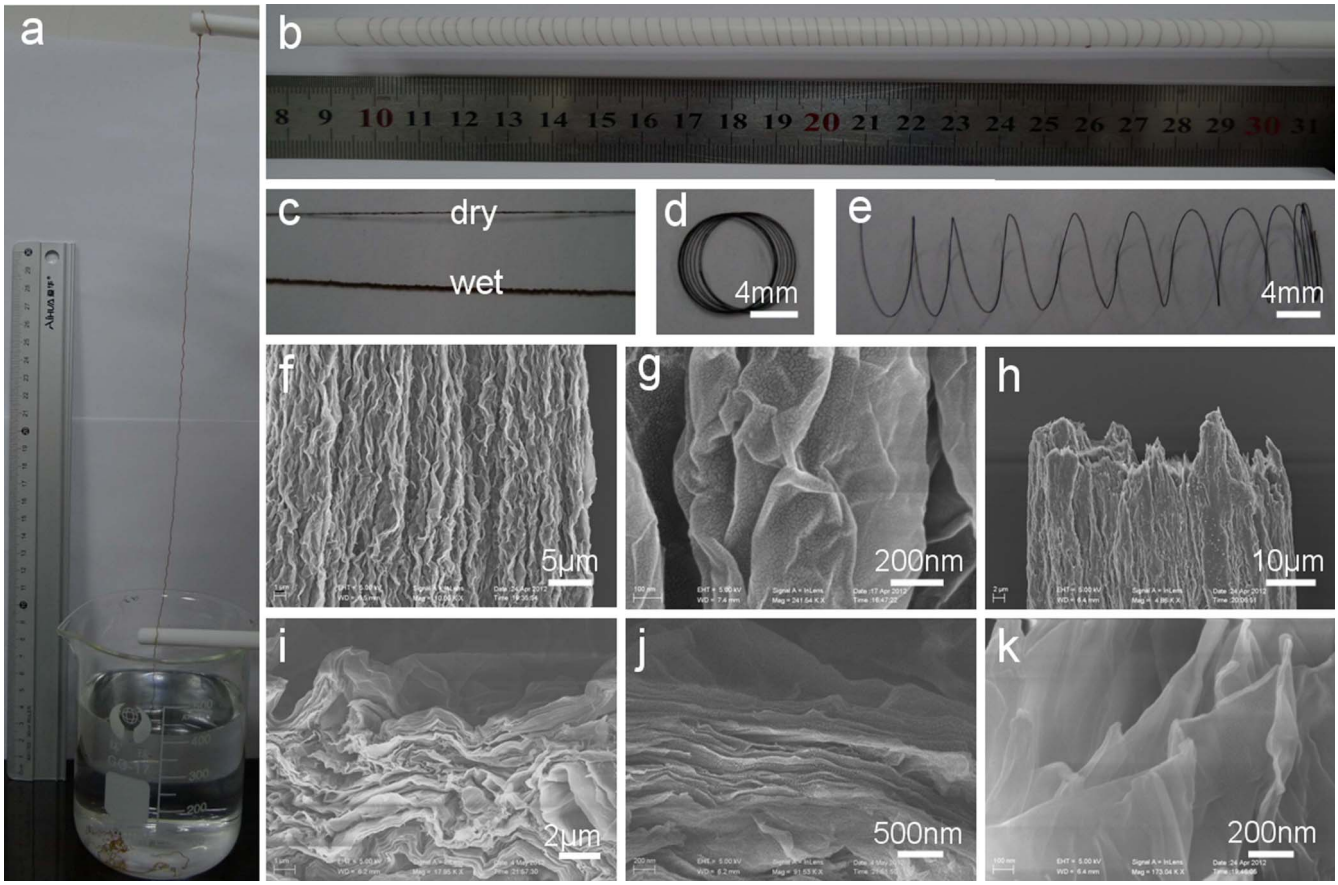

Figure 1 | Preparation and microstructures of macroscopic GO fibers. Photographs of (a) 50 cm-long fiber drawn out from the CTAB solution by wet spinning of the 10 mg/mL GO dopes in a coagulation bath of 0.5 mg/mL CTAB solution; (b) ~ 1.6 m-long fiber wound on a Teflon rod with a diameter of 8 mm; (c) the dry and wet fibers; (d) the fiber coil; (e) spring-like fiber by spreading out of coil in (d). (f, g) SEM images of the axial outer surface with different magnifications. (h–k) SEM images of the end of the broken part the fiber with different magnifications.

mechanical strength (~ 182 MPa), high electronic conductivity (~ 35 S/cm), and flexible multi-functionality just by *in situ* or post-synthesis integration of various functional nanomaterials into GO fibers.

Results

Wet-spinning of macroscopic GO fibers. The initially prepared GO dopes are well dispersed and composed of the thin GO nanosheets with a thickness of ~ 0.7 nm as presented in the AFM image and the corresponding height profile (see Supplementary Fig. S1 online). Then, for continuously producing neat GO fibers, the aqueous GO suspensions of 10 mg/mL are injected into the coagulation bath of 0.5 mg/mL CTAB solution by using a simple double-jet pump, from which two pieces of GO fibers are spouted out simultaneously (see Supplementary Fig. S2 online). It is a facile and viable strategy to fluidly spin the macroscopic GO fiber in a continuous and large-scale way. After injecting GO dopes into the coagulation bath, a ~ 1.6 meter-long GO fiber can be drawn out from the coagulation solution and wound on a Teflon rod directly, as shown in the photographs (Fig. 1a and 1b). Drawn from the solution, the dried fiber holds the same length as in its wet state, but with a significantly shrank diameter (Fig. 1c). After taking out of the dry fiber from the Teflon rod directly, the GO fiber coil can be pulled out to a perfect GO spring (Fig. 1d and 1e). Carried with a tweezers along the axial direction, the obtained GO spring still keeps its nice and stable state, disclosing its well stretchable and robust property (see Supplementary Fig. S3a online). Interestingly, the prepared dry GO fibers can be used as the threads to knit with a needle, shown from the knitted pattern of "USTC" letters in a cotton textile (see Supplementary Fig. S3b online).

Motivated by the attractive properties of the macroscopic GO fibers, SEM measurements are carried out detailedly to open out the characteristics of the microstructures (Fig. 1f–1k). SEM image (Fig. 1f) shows the high-order alignment of the densely-stacked GO sheets along the long axis. The thin GO nanosheets with abundant crumbled structures are observed from the outer surface of GO fiber, beneficial to the flexible property of the macroscopic fiber[23]. The SEM image of the end of the broken part (Fig. 1h) well verifies the assembly structures parallel to the axial direction. Furthermore, uniformly layered structures of the thin GO sheets are obviously revealed from the magnified SEM images of the end of the GO fiber (Fig. 1i–1k). From above analysis, it can be concluded that the ordered layered GO thin sheets are assembled to form the macroscopic fiber in a parallel-to-axis alignment.

Herein, one convenient advantage followed with the wet spinning technique is that the diameter of the macroscopic fiber can be controlled by changing the size of the nozzle or the concentration of the GO dope. The photograph shows the increasing trends of the diameters of the GO fibers in the coagulation solution with the sizes of the nozzles from 0.11, 0.26, 0.41, to 0.6 mm (see Supplementary Fig. S4a online). SEM images reveal the effectively tunable diameters of the GO fibers of 27, 45, 53 and 120 μm, corresponding to the concentrations of the GO dopes of 5, 8, 10, 22 mg/mL, respectively (see Supplementary Fig. S4b-S4e online).

Characterization and properties of chemically reduced graphene fibers. In order to get macroscopic graphene fibers, GO fibers are directly processed by the chemical reduction using hydroiodic acid as

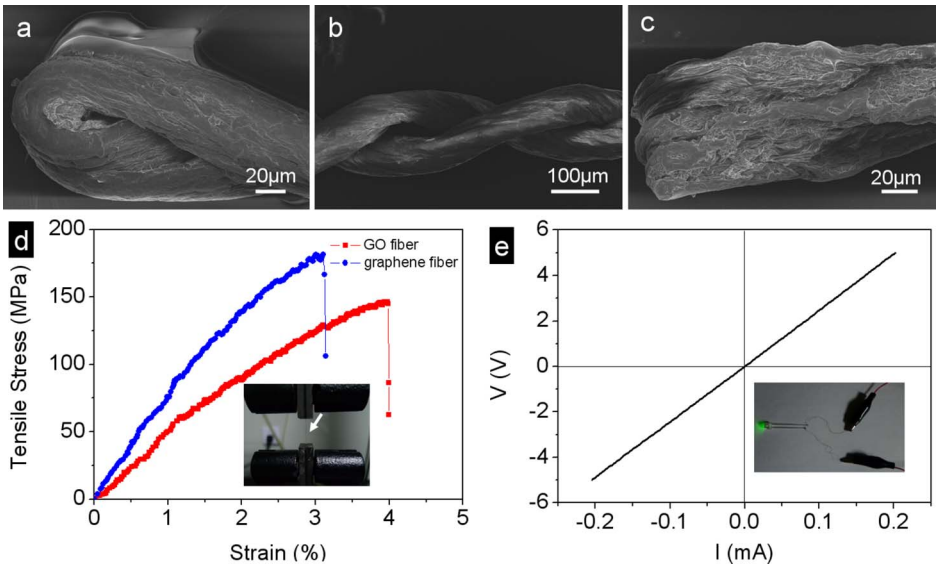

Figure 2 | Flexibility, mechanical and electrical properties of graphene fibers. SEM images of (a) the end of the twisted fiber; (b) the middle of the twisted fiber; (c) the end of the folded fiber. (d) Typical strain-stress curves of the single GO and graphene fiber. The inset photograph showing the testing state of the single fiber. (e) Typical I-V curve of the single graphene fiber with the length of 13.5 cm. The inset shows the lighted LED lamp using the prepared graphene fiber as the leads.

reducing agent[31]. As shown in the SEM images, the graphene fiber remains the order alignment of the curved thin sheets directional to the long axis (see Supplementary Fig. S5 online). However, the diameter of the reduced GO fiber decreases from 53 μm of GO fiber to 43 μm arising from the removal of oxygen-containing groups of GO[31]. High effectiveness of the reduction of the GO fiber to graphene fiber is confirmed by the Raman spectra (see Supplementary Fig. S6a and S6c online). The value of the intensity ratio of the characteristic D band (1353 cm^{-1}) and G band (1589 cm^{-1}) (I_D/I_G) of the graphene fiber, indicative as the degree of disorder and the average size of the sp^2 domains, increases to 1.1 in comparison with that of GO fiber of 0.9[32]. In addition, the 2D band at 2683 cm^{-1} in Raman spectra is strengthened after reduction, revealing the restoration of sp^2 carbon and the decrease of sp^3 carbon defects.

The obtained graphene fiber exhibits the intriguing flexibility and good resistance to torsion as shown from the SEM images (Fig. 2a–2c). Twisting or folding has no damage to the graphene fibers. The tensile strength and Young's modulus of the individual GO fiber displaced between two clamps are measured to 145 MPa and 4.2 GPa, respectively, and the corresponding elongation of which is about 4.0% (Fig. 2d). After reduced to graphene fiber, the tensile strength and Young's modulus have enhanced to 182 MPa and 8.7 GPa, respectively, due to the stronger interactions between the more compact stacks of the reduced GO sheets[23]. The tensile strength of the graphene fiber is higher than that of the neat wet-spinning single-walled carbon tube fibers (50–150 MPa)[26–27], owing to the high-order alignment and stretchable property of the thin sheets with the crumbled structures. The good electrical conductivity of ~ 35 S/cm of the graphene fiber is measured by the I–V curve (Fig. 2e), higher than the hydrothermally fabricated graphene fiber (10 S/cm). Using the prepared graphene fiber as the leads, the LED lamp can be lighted, as shown in the inset photograph of Fig. 2e. We expect that these macroscopic flexible graphene fibers with high mechanical strength and electrical conductivity can be woven into various objects alone or with other commercial threads together for the promising applications, such as blocking electromagnetic waves[28].

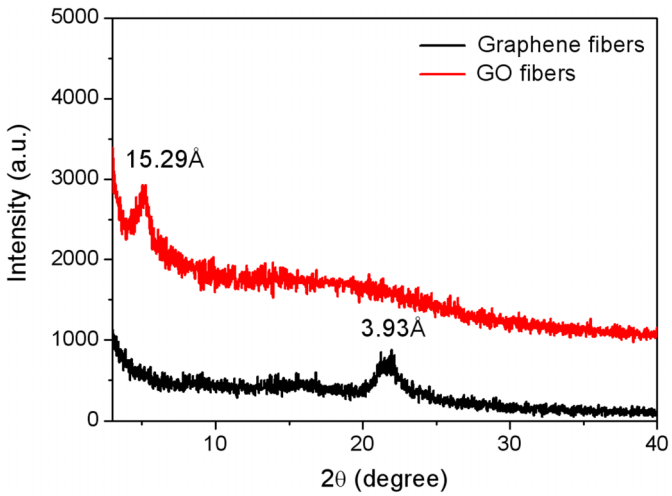

Figure 3 | XRD patterns of GO and graphene fibers.

Assembly mechanism of macroscopic GO fibers. In our wet-spinning method, CTAB solution is chosen as the coagulation bath due to its positive charge which may play a surprising role in the assembly of the negative-charged GO suspension. XRD pattern of GO fibers in Fig. 3 shows a sharp diffraction peak at 2θ position of 5.07°, corresponding to the interlayer spacing of 15.29 Å. Compared with the interlayer spacing of the ordered GO assemblies reported in the literatures (8–9 Å)[23,31], the much larger value herein reveals the lamellar structures involving in the electrostatic interactions between CTAB molecules and GO sheets during the formation of GO fibers. After reduced to graphene fibers, CTAB molecules are removed from the fibers due to the significant decrease of electrostatic attractions followed with GO reduced to graphene sheets, which is reflected from the small interlayer spacing of 3.93 Å (2θ = 21.98°) for the XRD pattern of graphene fibers.

Meanwhile, the assembly process of the macroscopic GO fiber is vividly detected at the low CTAB concentration of 0.05 mg/mL. The low-magnified SEM image in Fig. 4Aa shows an unripe GO fiber with several sections just because of not high enough concentration of CTAB, strongly revealing the evolution process of the formation of

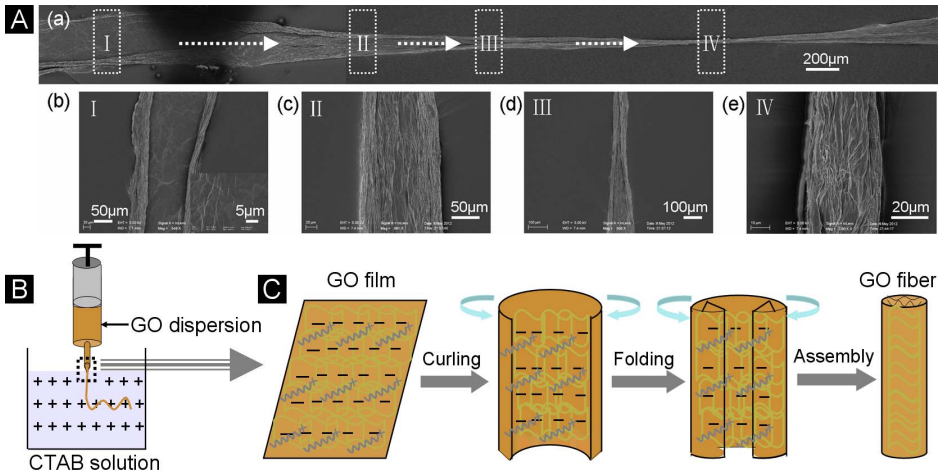

Figure 4 | Formation mechanism of the GO fiber. (A) SEM images illustrating the assembly process of the GO fiber by spinning 10 mg/mL of GO dopes into CTAB coagulation solution of 0.05 mg/mL. (a) A single GO fiber. (b–e) Magnified SEM images corresponding to the different parts of the single fiber of (a). (B) Schematic illustration of the typical apparatus of wet-spinning GO fibers. (C) Schematic illustration of the assembly mechanism of the GO fiber.

GO fiber. Careful observations through high magnifications of SEM images are made on the four distinctive sections of the same GO fiber marked with the rectangular frames (Fig. 4Ab–4Ae). At the beginning of the GO dopes injected into the coagulation bath, a multilayer film of GO sheets with a diameter of about 245 μm is produced, owing to the strong repulsions between the negative-charged GO sheets (stage I). Due to the charge neutralizations between CTAB and GO, the weakened electrostatic repulsions make the edges of GO film curling and folding towards the center, resulting in a directionally-aligned belt in a 130 μm diameter (stage II). Following with repeated cycles of curliness and fold arising from the further neutralizations of the electrostatic repulsions between GO sheets, the diameter of the GO is reduced gradually up to form a neat GO fiber with the high-order alignment along the main axis (stage III and IV).

From above analysis based on the XRD and SEM observations, CTAB plays a crucial role in the evolution process of the GO fiber. Compared with the GO powder, the FT-IR spectrum of the as-fabricated GO fiber exhibits a group of bands at 2960, 2920, 2845, 1285, and 720 cm^{-1}, corresponding to υ_{as}-CH_3, υ_{as}-CH_2, υ_s-CH_2, υ-(C-N) and γ-(C-C) of the characteristic bands of CTAB, respectively (see Supplementary Fig. S7a online). Furthermore, the XPS spectrum of the GO fiber shows the N1s peak at 402 eV with the content of 2.94 at.% (see Supplementary Fig. S7b online). These data confirm the incorporation of CTAB into the final GO fiber resulting from the electrostatic attractions during the assembly process.

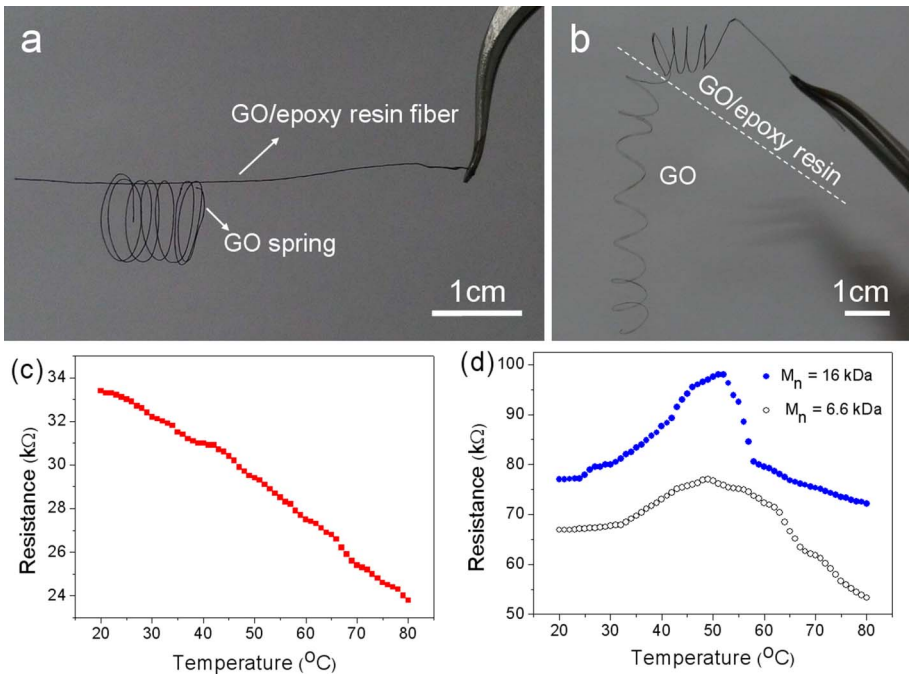

Figure 5 | Multifunctionalization of the macroscopic graphene-based fibers. Photographs of (a) a GO/epoxy resin fiber supporting a GO spring; (b) a spring with two halves, one the GO/epoxy resin fiber, the other GO fiber. The GO/epoxy resin fiber was prepared by soaking the GO fiber of 10 mg/mL into epoxy resin solution followed with thermal solidification. (c) Curve of resistance change with temperature of a single graphene fiber. (d) R-T curves of a single graphene/PNIPAM composite fiber by wet-spinning of GO-PNIPAM dopes followed with chemical reduction (GO suspensions of 5 mg/mL, the weight ratio of GO and PNIPAM of 1:1). Two kinds of molecular weights of PNIPAM were used (16 kDa and 6.6 kDa).

Multifunctionalization of macroscopic graphene-based fibers. Another attractive advantage of the wet-spinning technique mentioned here is that it is well-suited to fabricate the functionalized graphene-based fibers combined with the in-situ or post-synthesis strategy. Herein, the flexible GO fiber can be easily processed into the rigid one. If the pre-fabricated GO fiber is soaked with the epoxy resin solution followed with thermal solidification, the fiber with good rigidity can be obtained, as shown from a GO/epoxy resin fiber supporting the GO spring in the photograph of Fig. 5a. Furthermore, it is convenient to get the GO/epoxy resin fibers with changeful configurations just dipping the pre-designed GO fibers into the epoxy resin solution. The photograph of Fig. 5b displays a piece of spring with two halves, one half the rigid GO/epoxy resin fiber and the other the flexible GO fiber. The low-magnified SEM images (see Supplementary Fig. S8a and S8b online) show the slippery surface of the GO/epoxy resin fiber with an increased diameter of $\sim$ 120 μm. Furthermore, the lamellar structures of epoxy resin and GO sheets are observed from the magnified SEM images of the cross section of the broken GO/epoxy resin fiber, well revealing the incorporation of epoxy resin into the inner of GO fiber, not only the coverage outside of the surfaces. Due to the thick incorporation of epoxy resin in the inner and outer of GO fiber, a wide diffraction peak centered at 17.9° is shown in the XRD pattern (see Supplementary Fig. S9a online). The high Young's modulus of 6.73 GPa and the low elongation strain of 1.24% reveal the rigid characteristic of the GO/epoxy resin fiber (see Supplementary Fig. S9b online).

The facile manipulation to functionalize the GO fibers is not only limited to the pre-prepared fibers. Taking the typically thermosensitive polymer, poly(N-isopropylacrylamide) (PNIPAM), for an example, the GO/PNIPAM fiber keeps an ordered alignment along the long axis (see Supplementary Fig. S10a and S10b online), when dissolving PNIPAM powders into the GO dopes of 5 mg/mL with the weight ratio of 1:1 followed with the typical wet-spinning process. The diameter of the GO/PNIPAM fiber is increased to 55 μm arising from the successful incorporation of the PNIPAM polymer into the fibers, compared with that of the GO fiber of 27 μm with the identical concentration mentioned above. Furthermore, the FT-IR spectra of the single GO and GO/PNIPAM fiber confirm the existence of the polymer in the fiber, as reflected from the characteristic bands belonging to PNIPAM (see Supplementary Fig. S11 online)[33]. After treated with HI, the GO/PNIPAM fiber is reduced to graphene/PNIPAM fiber as shown from the improved value of I_D/I_G and the existence of 2D band of the Raman spectra (see Supplementary Fig. S6b and S6d online). The reduced fiber holds the aligned structure with a decreased diameter of 47 μm (see Supplementary Fig. S10c and S10d online).

Interestingly, the distinctively thermosensitive property is possessed with the graphene/PNIPAM fiber originating from the integration of PNIPAM into the graphene fiber. As shown in Fig. 5c, the resistance of the graphene fiber is decreased linearly with the rise of the temperature in the range of 20–80°C. As to the resistance-temperature (R-T) curves of the graphene/PNIPAM fibers in Fig. 5d, the resistance is initially increased with the higher temperature due to the shrinkage of the diameter of the fiber arising from the continuous phase transition of PNIPAM above the critical temperature, known as the lower critical solution temperature (LCST)[34]. After finishing the phase transition of PNIPAM, the resistance of the fiber with the improved temperature has a descending trend coming of the characteristic of the graphene fiber. Thus, it can be seen that the resistance of the composite fiber is affected by two opposite actions with the rising temperatures: the phase transition-induced increase by PNIPAM and the nature decrease by graphene. In the first stage, the former plays the dominant role and the reverse for the second stage. Therefore, the R-T curves of graphene/PNIPAM fibers with different molecular weights (MW) show the similar trends. However, the change of the resistance of the graphene/PNIPAM fiber with low MW is not as sharp as that of the high MW PNIPAM due to the broader range of the phase transition of the low MW PNIPAM[35]. The tunable thermo-responses of the interesting graphene/PNIPAM fibers indicate the promising applications for the thermosensitive devices.

Not only various polymers, but also inorganic nanomaterials can be integrated into GO fibers conveniently, resulting in the enhanced properties or new functionalities for macroscopic fibers. Just as shown from the SEM images (see Supplementary Fig. S12a and S12b online), the multi-walled carbon nanotubes (MWCNTs) have spun with the GO dopes simultaneously with the weight ratio of GO and MWCNTs of 2:1, exhibiting the ordered multilayered structures between GO sheets and MWCNTs. Importantly, the tensile strength of the obtained GO/MWCNTs fiber can be adjusted by changing the weight ratio of GO and MWCNTs. With the integration of MWCNTs into the GO fibers, the mechanical strengths are enhanced to 180 and 220 MPa, corresponding to the weight ratio of GO and MWCNTs of 3:1 and 2:1, respectively. However, too high amount of MWCNTs incorporated damages the mechanical property of the macroscopic fibers arising from the less-efficiency assembly of GO fibers, reflected from the typical stress-strain curve (see Supplementary Fig. S12c online). From these vivid examples of functionalization, it is reasonable to believe that various organic or inorganic materials with novel morphology and specific functionalities can be engineered into the macroscopic graphene-based fibers with high mechanical strength and electrical conductivity for diverse practical applications.

Discussion

According to the characterizations of the microstructures and components referred in the evolution process of the GO fibers, the formation mechanism of the macroscopic fiber is described by schematic illustrations as shown in Fig. 4B and Fig. 4C. Since the GO dopes injected into the positive-charged CTAB solution, as sketched in Fig. 4B, the electrostatic interaction-induced assembly between GO nanosheets and CTAB molecules occurs quickly. Initially, a piece of the GO thin film spreads out in the coagulation solution mainly due to the electrostatic repulsions between the negative charges that GO contains. Then, owing to the charge neutralization, the CTAB molecules continuously adsorbed on the thin film make the repulsions between GO sheets weakened. Thus, the formed thin film starts to curl from the two edges towards the center. More and more adsorptions of CTAB result in the significant curliness of the two edges in a respectively folio way. Following with repeated curling-folding process of the thin film, the neat GO fibers are produced, with CTAB molecules incorporated into the GO sheets, forming hierarchically lamellar structure. In this way, the positive-charged CTAB as the coagulation solution induces the assembly of the macroscopic GO fiber in a high-order manner.

In summary, the neat, flexible, and macroscopic graphene fibers have been continuously fabricated by a convenient wet-spinning technique followed with the highly-efficient chemical reduction in large scale. We firstly expose the curliness-fold mechanism for the assembly of the GO fiber under the electrostatic interactions of the opposite charges. The facile integration of various functional guest materials into the graphene host endows the graphene-based fibers with the hierarchical microstructures and the new or enhanced properties, which lays the solid foundations for exploring the potential applications in the fields of high-performance sensors, energy storages and catalysts *etc*.

Methods

Preparation of GO and graphene fibers. GO sheets were prepared by the chemical oxidation of graphite flakes (Sigma-Aldrich) according to the modified Hummers method reported previously[36]. In a typical fabrication of GO fiber, the 10 mg/mL of the degassed GO dopes were loaded in the plastic syringe and injected into the CTAB coagulation bath of 0.5 mg/mL with the injection pump. The obtained GO fibers were washed, and then dried at room temperature after taking out from the solution.

Hydroiodic acid (40 %) was used to reduce GO fiber to graphene fiber at 80°C overnight.

Preparation of GO/epoxy resin fibers. The pre-fabricated GO fibers were soaked into the epoxy resin acetone solution with the weight ratio of epoxy resin and 4, 4′-Diaminodiphenylmethane of 2:1 for 8 h. Then, the fibers were taken out, transferred in a Teflon plate and placed in an oven to solidify at 100°C for 2 h and 150°C for 2 h.

Preparation of GO/PNIPAM fibers. PNIPAM powder was dissolved into the GO suspension of 5 mg/mL with the weight ratio of 1:1 under stirring. After degassed, the GO/PNIPAM fibers were prepared by the wet-spinning method mentioned above. The graphene/ PNIPAM fibers were prepared by the chemical reduction with HI (40%) at room temperature for 24 h.

Preparation of GO/MWCNTs fibers. The commercial MWNCTs pre-treated with nitric acid[37] were mixed with GO dopes with the weight ratio of GO and MWCNTs of 2:1 under stirring overnight. And then, the degassed GO-MWCNTs dopes were spun by the similar procedure mentioned above.

Instruments. Scanning electron microscope (SEM) images were performed on a field emission scanning electron microanalyzer (Zeiss Supra 40) at an acceleration voltage of 5 kV. Atomic force microscope (AFM) image was carried out on a Multimode V (VEECO) under contact mode. Raman spectra were conducted on a confocal laser microRaman spectrometer (LABRAM-HR, JY Co.) FTIR spectra were recorded on a Bruker Vector-22 FTIR spectrometer from 4000–400 cm^{-1}. X-ray photoelectron spectrum (XPS) was tested on an ESCALab MKII X-ray photoelectron spectrometer using Mg Ka radiation exciting source. The tensile stress-strain test for the single fiber was measured by using Instron 5565A. The electrical conductivity of the single graphene-based fiber was measured by a two-probe method with PM5 Analytical Probe System (Cascade Microtech, Inc.) and Keithley 4200 SCS. For testing the GO/PNIPAM fiber, the single fiber was connected with two pieces of the copper wires with silver paste (Dupont 4929N) and soaked in heated ultrapurified water (18.2 MΩ).

1. Geim, A. K. & Novoselov, K. S. The rise of graphene. *Nature Mater.* **6**, 183–191 (2007).
2. Novoselov, K. S. *et al*. Electric field effect in atomically thin carbon films. *Science* **306**, 666–669 (2004).
3. Geim, A. K. Graphene: Status and prospects. *Science* **324**, 1530–1534 (2009).
4. Stoller, M. D., Park, S. J., Zhu, Y. W., An, J. H. & Ruoff, R. S. Graphene-based ultracapacitors. *Nano Lett.* **8**, 3498–3502 (2008).
5. Oh, D. Y. *et al*. Graphene sheets stabilized on genetically engineered m13 viral templates as conducting frameworks for hybrid energy-storage materials. *Small* **8**, 1006–1011 (2012).
6. Robinson, J. T., Perkins, F. K., Snow, E. S., Wei, Z. Q. & Sheehan, P. E. Reduced graphene oxide molecular sensors. *Nano Lett.* **8**, 3137–3140 (2008).
7. Deng, S. *et al*. Reduced graphene oxide conjugated cu2o nanowire mesocrystals for high-performance no2 gas sensor. *J. Am. Chem. Soc.* **134**, 4905–4917 (2012).
8. Long, J. L. *et al*. Nitrogen-doped graphene nanosheets as metal-free catalysts for aerobic selective oxidation of benzylic alcohols. *Acs Cataly.* **2**, 622–631 (2012).
9. Xue, T. *et al*. Graphene-supported hemin as a highly active biomimetic oxidation catalyst. *Angew. Chem. Int. Ed.* **51**, 3822–3825 (2012).
10. Huang, X., Qi, X. Y., Boey, F. & Zhang, H. Graphene-based composites. *Chem. Soc. Rev.* **41**, 666–686 (2012).
11. Li, T. *et al*. Solution-processed ultrathin chemically derived graphene films as soft top contacts for solid-state molecular electronic junctions. *Adv. Mater.* **24**, 1333–1339 (2012).
12. Liang, M. H., Wang, J., Luo, B., Qiu, T. F. & Zhi, L. J. High-efficiency and room-temperature reduction of graphene oxide: A facile green approach towards flexible graphene films. *Small* **8**, 1180–1184 (2012).
13. Zhang, L. L. *et al*. Highly conductive and porous activated reduced graphene oxide films for high-power supercapacitors. *Nano Lett.* **12**, 1806–1812 (2012).
14. Seo, S. *et al*. Solution-processed reduced graphene oxide films as electronic contacts for molecular monolayer junctions. *Angew. Chem. Int. Ed.* **51**, 108–112 (2012).
15. Kwak, J. *et al*. Near room-temperature synthesis of transfer-free graphene films. *Nat. Commun.* **3**, 645 (2012).
16. Cote, L. J., Cruz-Silva, R. & Huang, J. Flash reduction and patterning of graphite oxide and its polymer composite. *J. Am. Chem. Soc.* **131**, 11027–11032 (2009).
17. Vickery, J. L., Patil, A. J. & Mann, S. Fabrication of graphene-polymer nanocomposites with higher-order three-dimensional architectures. *Adv. Mater.* **21**, 2180 (2009).
18. Cai, D. & Song, M. Recent advance in functionalized graphene/polymer nanocomposites. *J. Mater. Chem.* **20**, 7906–7915 (2010).
19. Xu, Y., Sheng, K., Li, C. & Shi, G. Self-assembled graphene hydrogel via a one-step hydrothermal process. *Acs Nano* **4**, 4324–4330 (2010).
20. Chen, W. & Yan, L. In situ self-assembly of mild chemical reduction graphene for three-dimensional architectures. *Nanoscale* **3**, 3132–3137 (2011).
21. Tang, Z., Shen, S., Zhuang, J. & Wang, X. Noble-metal-promoted three-dimensional macroassembly of single-layered graphene oxide. *Angew. Chem. Int. Ed.* **49**, 4603–4607 (2010).
22. Cong, H.-P., Ren, X.-C., Wang, P. & Yu, S.-H. Macroscopic multifunctional graphene-based hydrogels and aerogels by a metal ion induced self-assembly process. *Acs Nano* **6**, 2693–2703 (2012).
23. Xu, Z. & Gao, C. Graphene chiral liquid crystals and macroscopic assembled fibres. *Nat. Commun.* **2** (2011).
24. Dong, Z. *et al*. Facile fabrication of light, flexible and multifunctional graphene fibers. *Adv. Mater.* **24**, 1856–1861 (2012).
25. Dalton, A. B. *et al*. Super-tough carbon-nanotube fibres - these extraordinary composite fibres can be woven into electronic textiles. *Nature* **423**, 703–703 (2003).
26. Ericson, L. M. *et al*. Macroscopic, neat, single-walled carbon nanotube fibers. *Science* **305**, 1447–1450 (2004).
27. Davis, V. A. *et al*. True solutions of single-walled carbon nanotubes for assembly into macroscopic materials. *Nature Nanotech.* **4**, 830–834 (2009).
28. Jiang, K. L., Li, Q. Q. & Fan, S. S. Nanotechnology: Spinning continuous carbon nanotube yarns - carbon nanotubes weave their way into a range of imaginative macroscopic applications. *Nature* **419**, 801–801 (2002).
29. Li, Y. L., Kinloch, I. A. & Windle, A. H. Direct spinning of carbon nanotube fibers from chemical vapor deposition synthesis. *Science* **304**, 276–278 (2004).
30. Zhang, M., Atkinson, K. R. & Baughman, R. H. Multifunctional carbon nanotube yarns by downsizing an ancient technology. *Science* **306**, 1358–1361 (2004).
31. Pei, S., Zhao, J., Du, J., Ren, W. & Cheng, H.-M. Direct reduction of graphene oxide films into highly conductive and flexible graphene films by hydrohalic acids. *Carbon* **48**, 4466–4474 (2010).
32. Stankovich, S. *et al*. Synthesis of graphene-based nanosheets via chemical reduction of exfoliated graphite oxide. *Carbon* **45**, 1558–1565 (2007).
33. Kurz, V., Grunze, M. & Koelsch, P. In situ characterization of thermo-responsive poly(n-isopropylacrylamide) films with sum-frequency generation spectroscopy. *Chemphyschem* **11**, 1425–1429 (2010).
34. Schild, H. G. Poly (n-isopropylacrylamide) - experiment, theory and application. *Prog. Polym. Sci.* **17**, 163–249 (1992).
35. Xia, Y., Burke, N. A. D. & Stover, H. D. H. End group effect on the thermal response of narrow-disperse poly(n-isopropylacrylamide) prepared by atom transfer radical polymerization. *Macromolecules* **39**, 2275–2283 (2006).
36. Zhao, G. *et al*. Synthesizing mno2 nanosheets from graphene oxide templates for high performance pseudosupercapacitors. *Chem. Sci.* **3**, 433–437 (2012).
37. Datsyuk, V. *et al*. Chemical oxidation of multiwalled carbon nanotubes. *Carbon* **46**, 833-840 (2008).

Acknowledgments

S.-H. Y. acknowledges the funding support from the National Basic Research Program of China (2010CB934700), the National Natural Science Foundation of China (Nos. 91022032, 21061160492, J1030412), the Chinese Academy of Sciences (Grant KJZD-EW-M01-1), International Science & Technology Cooperation Program of China (2010DFA41170), the Principal Investigator Award by the National Synchrotron Radiation Laboratory at the University of Science and Technology of China. H.-P.C. thanks the National Natural Science Foundation of China (Nos. 21001099), the Fundamental Research Funds for the Central Universities, China Postdoctoral Science Foundation (20110490086), and the Foundation for the Author of Excellent Doctoral Dissertation of CAS. We thank Dr. Xiao-Dong Ye and Prof. Guang-Ming Liu in Department of Chemical Physics of USTC for the synthesis of PNIPAM and the beneficial discussions.

Author contributions

H.-P.C. planned and performed the experiments, collected and analyzed the data, and wrote the paper. S.-H.Y. supervised the project, and conceived the experiments, analyzed the results and wrote the paper. X.-C.R. and P.W. helped with synthesis of the materials and collected the data. All authors discussed the results and commented on the manuscript.

Additional information

Supplementary information accompanies this paper at http://www.nature.com/scientificreports

Competing financial interests: The authors declare no competing financial interests.

How to cite this article: Cong, H.-P, Ren, X.-C, Wang, P. & Yu, S.-H Wet-spinning assembly of continuous, neat, and macroscopic graphene fibers. *Sci. Rep.* **2**, 613; DOI:10.1038/srep00613 (2012).